Journal of Magnetic Resonance 197 (2009) 56–62

Contents lists available at ScienceDirect

Journal of Magnetic Resonance

journal homepage: www.elsevier.com/locate/jmr

Resolution enhancement in MRI of laser polarized ^{3}He by control of diffusion

L. Agulles-Pedrós [1], R.H. Acosta [2], P. Blümler [*,3], H.W. Spiess

Max Planck-Institute for Polymer Research, Ackermannweg 10, 55128 Mainz, Germany

ARTICLE INFO

Article history:
Received 24 September 2008
Revised 3 December 2008
Available online 13 December 2008

Keywords:
Gas MRI
Restricted diffusion
Edge enhancement
Motional averaging
Contrast
Hyperpolarized gases

ABSTRACT

Diffusion of atoms or molecules in presence of magnetic field gradients not only attenuates the NMR signal but also leads to distortions close to restricting boundaries. This phenomenon is most evident in imaging with laser polarized (LP) noble gases. Diffusion of gases can be manipulated, however, by admixing inert gases of different molecular weight. In this work we analyze the effect of mixing LP-^{3}He with SF_6 on the image quality of a phantom consisting of an arrangement of capillaries with different diameters. Admixing buffer gases of higher molecular weight changes the contrast and offers a means to record images with high spatial and time resolution. Additionally we demonstrate how distortions due to edge enhancement can be reduced even for long timed MRI-sequences.

1. Introduction

NMR studies of laser polarized (LP) gases received considerable attention in the last decade. Laser polarization circumvents the low thermal polarization of gases and can yield exceedingly high magnetizations, especially for ^{3}He and ^{129}Xe. Compared to conventional thermal signal sources LP gases provide magnetization that is independent of the external magnetic field and does not recover thermally. For instance, the achievable polarization of LP-^{3}He can exceed 60% (experimentally obtained maximum: 92% [1]) giving rise to extremely high magnetization. Thus, even for rf-pulses with tip angles in the range of 5°, very good signal to noise ratios (SNR) can be obtained and with a single batch of gas a large number of acquisitions can be performed in an imaging experiment [2–4]. A drawback of MRI with LP gases, however, is the very high diffusion coefficient of gases, up to five orders of magnitude higher than in liquids. The rapid Brownian motion strongly attenuates the NMR signal in the presence of static field gradients which severely restricts the achievable spatial resolution [5]. Recently we have shown that the fast spatial diffusion in LP-^{3}He can even interfere with the formation of a simple Hahn echo, yielding an echo maximum at $\sqrt{2}\tau$ rather than at 2τ, where τ is the pulse spacing [6]. Moreover, diffusion can mask subtle effects such as the presence of distant dipolar fields in gases [7,8]. Imaging not only implies the use of gradients but also that the sample consists of structures which should be resolved, hence the presence of spatial restrictions. Depending on their size, such structures will reduce the mean free path a molecule can travel during the experimental lifetime giving rise to a much lower apparent diffusion coefficient (ADC) [9]. This in turn will generate a contrast in MRI which depends on the cavity sizes. For gases in particular, the determination of diffusion coefficients in restricted media has been successfully employed to probe the microscopic structure and functionality in lungs [4,10,11] and time dependent diffusion coefficient measurements were shown to give structural information on porous media [12–15]. The usual experimental approaches exploit the fact that short and weak gradients maximize the SNR on bigger cavities, where the ADCs will lead to a stronger attenuation of the signal.

Manipulation of the diffusion coefficient of the gas provides an alternative to control signal intensity and contrast. At first sight this may seem to be a drawback for experiments in which the variation in ADC can be correlated to a change in local pore size, as in the case of lung emphysema [4]. The strongly restricted diffusion in the alveoli will be more difficult to observe when the LP-^{3}He is in a mixture with a heavy buffer gas. However, an increase in the SNR could allow a faster determination of the ADC, and become very useful in clinical MRI schemes. Recently we presented an experimental protocol which allows the precise determination of gas mixtures and the control of the diffusion coefficient of ^{3}He for a wide range of concentrations with different buffer gases [9].

* Corresponding author. Fax: +49 2461 61 2492.
E-mail addresses: p.bluemler@fz-juelich.de (P. Blümler), bluemler@mpip-mainz.mpg.de (P. Blümler).
[1] Present address: Pontificia Universidad Javeriana Bogotá, Facultad de Ciencias, Depto. Física, Cr 7ª # 45 Bogotá, Colombia.
[2] Present address: Facultad de Matemática, Astronomía y Física, Universidad Nacional de Córdoba, X5016LAE Córdoba, Argentina.
[3] Present address: Institute of the Chemistry and Dynamics of the Geosphere, ICG-3: Phytosphere, Forschungszentrum Jülich, 52425 Jülich, Germany.

1090-7807/$ - see front matter © 2008 Elsevier Inc. All rights reserved.
doi:10.1016/j.jmr.2008.12.003

Gas mixtures were then related to the obtainable signal attenuation and it was shown that for certain conditions an optimum gas mix can be chosen to obtain maximum NMR signals for unrestricted diffusion [16]. Preliminary results have been obtained on a dried mouse lung [17] where a mixture of LP-^{129}Xe and ^{3}He was imaged, showing a substantial increase of SNR of the trachea as compared to an image of pure helium [18]. In another experiment, the influence of using different buffer gases, such as ^{4}He, N_2 and SF_6 for diffusion weighted images of ^{3}He in the mixture was demonstrated in a dead pig's lung [16].

In order to resolve structures, boundaries must be introduced or present, and phenomena such as edge enhancement and motional narrowing must be taken into consideration [19–22]. Diffusion of a gas mix in restricted geometries becomes more complex as the restricted diffusion is determined by the size of the pore, the gas mix concentration and the observation time. In this work we analyze the sensitivity and resolution achievable for restricted gas diffusion in binary gas mixtures by comparing 2D images of a mixture of LP-^{3}He with SF_6 in a phantom consisting of capillaries with varying dimensions with pure helium images of the same phantom. We show how an improvement of the resolution of a 2D image can be obtained by reducing the diffusion coefficient in gas mixtures. Additionally, it is shown how the image quality can be improved by reducing edge enhancement and motional narrowing artifacts.

2. Theoretical background

2.1. Diffusion limited sensitivity and resolution

Due to the very high diffusion coefficients in gases even simple MR-images are strongly diffusion weighted [16]. In the case of a simple gradient echo sequence without additional diffusion gradients as schematized in Fig. 1, the signal attenuation, E, due to diffusion in the read direction is related to the experimental b-value [23],

$$\ln\frac{S(b)}{S(0)} = \ln E(b) = -bD \quad \text{with} \quad b = \gamma^2 G^2 \delta^2 \left(\Delta - \frac{\delta}{3}\right), \tag{1}$$

where γ denotes the magnetogyric ratio, G the gradient strength, δ the duration of a gradient pulse, Δ a delay between the starting points of the bipolar gradient pulses and S the NMR signal intensity. Between excitation and detection in one dimension (along the direction of the gradient) the mean square displacement of the diffusing spins is $\langle r^2\rangle = 2D(\delta + \Delta)$. As we deal with cylindrical restrictions, $\tilde{r}$ is a one-dimensional variable that ranges from $-\tilde{R}_i$ to $+\tilde{R}_i$,

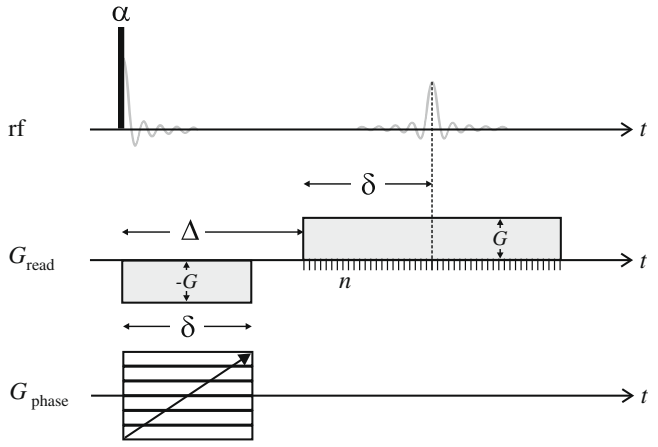

Fig. 1. Sketch of the pulse sequence used for 2D imaging labeled as described in the text. Top row: timing of rf excitation and detection; middle row: read or frequency encoding gradient; bottom row: phase encoding gradient.

with $\tilde{R}_i$ being the radius of the ith capillary. For the present experiments $\delta = \Delta$ rendering

$$\langle r^2\rangle = 4D\delta. \tag{2}$$

In a situation where there are restrictions on the free displacement of the spins, the time during which the phase of the spins is influenced by free diffusion can be used to define a critical size, $\tilde{r}_c = \sqrt{4D_0\delta}$, in which no borders are encountered. D_0 is the free diffusion coefficient. For a cavity with radius smaller than $\tilde{r}_c$ the apparent diffusion coefficient (ADC) is determined by the void size and for all voids with bigger diameters the diffusion is essentially free. The diffusion coefficient D is then a function of both, the cavity size and the timing of the sequence. Because this work focuses on the influence of diffusion in the presence of imaging gradients, only, D can be expressed as

$$D(\tilde{r},\delta) = \begin{cases} \text{ADC} = \frac{\langle r^2\rangle}{4\delta} & \text{for } r < \tilde{r} < \tilde{r}_c \\ D_0 & \text{for } \tilde{r} > \tilde{r}_c \end{cases}. \tag{3}$$

The behavior of D in the presence of restrictions as a function of time is a well studied problem and generally used to obtain information on the surface to volume ratio [15,24,25]. Although, Eq. (3) presents two limiting cases there is usually only a smooth transition between them observable.

Following Eq. (1) the influence of diffusion on the signal is usually minimized by making δ and Δ as short as technical and safety limits allow. However, the gradient strength is predetermined by the necessary field of view (FOV) to place n points across the sample or the required k-space trajectories. From this a spatial resolution, Δr, can be defined (ignoring influences of the line width and data post-processing) for the read direction

$$\text{FOV} = \frac{2\pi n}{\gamma G\delta} \quad \text{and} \quad \Delta r = \frac{\text{FOV}}{n} = \frac{2\pi}{\gamma G\delta} \tag{4}$$

This puts a very stringent limit on the achievable spatial resolution for MRI in the gas phase, as it becomes evident when Eqs. (2) and (4) are substituted into Eq. (1)

$$\ln E = -\frac{2}{3}\gamma^2 G^2 \delta^3 D = -\frac{2\pi^2\langle r^2\rangle}{3(\Delta r)^2} \tag{5}$$

This means that if a spatial resolution, Δr much below this critical size ($\Delta r^2 < \langle r^2\rangle \leqslant \tilde{r}_c^2$) is sought, the signal in Eq. (5) will vanish rapidly, i.e. the pore cannot be resolved. A way out of this dilemma is to change the critical radius or, equivalently D_0 by admixing buffer gases.

On the other hand, in the phase encoding direction the k-space is traversed by stepping up the gradient G_{phase} ($-G \leqslant G_{\text{phase}} < G$) while keeping its duration δ constant (cf. Fig. 1). The attenuation due to phase encoding for each signal is then

$$A(g,D) = \exp\left(-\frac{1}{3}\gamma^2 G^2 \delta^3 D\right). \tag{6}$$

After Fourier transformation (FT) this corresponds to a convolution of the image signals with the FT of this attenuation function, without further attenuation of the image intensity. Hence, only for very high diffusion coefficients or very small structures a blurring with a Gaussian along this direction will be obtained. This behavior has been treated in detail in terms of fast and slow exchange limits and is outlined in the next section.

2.2. Edge enhancement

The influence of borders in gas MRI is usually described in terms of edge enhancement and motional narrowing, or weak and strong diffusion regimes [19–22]. The parameter that characterizes these

regimes, as defined by de Swiet and Sen [20] is the diffusion length $l_g = \sqrt[3]{D/\gamma G}$. The limit when l_g is much larger than the dimension (l_s) of the distance defined by the restrictions along the direction of the gradient is the strong diffusion regime and gives rise to a motional narrowing. In this case a spin loses the memory of the initial position giving rise to an averaged frequency and a Lorentzian line. When $l_g \ll l_s$ (weak diffusion regime or edge enhancement) a stronger signal is observed near the edges where the motion is restricted. In the middle of the sample the attenuation due to diffusion follows Eq. (1).

In the case of phase encoding the strong diffusion regime is defined by $l_g^{phase} = \sqrt{D\delta} \gg l_s$. In this regime, it has been shown by de Swiet [21] that, in contrast to the Lorentzian line in the frequency-encoded direction, a Gaussian will be obtained.

3. Materials and methods

Data were acquired in a 4.7 T horizontal, 20 cm bore magnet (Magnex Scientific Ltd, UK) equipped with actively shielded gradients (capable of producing gradients up to 0.3 T m^{-1}) from Bruker (Bruker Biospin GmbH, Germany). The gradients were driven by amplifiers from Copley (Copley Controls Corp., USA). A birdcage-coil of 21 mm inner diameter and 37 mm length from Bruker was used for rf excitation and detection at a frequency of 153 MHz for ^{3}He. The gradients and the rf were controlled from a Maran DRX console (Oxford Instruments Ltd, Witney, UK) controlled within a Matlab (MathWorks Inc., USA) environment with homemade software. The ^{3}He polarization was generated with a home built large scale polarizer at the department of Physics in the University of Mainz, which can routinely produce up to 70% of polarization at 3.3 bar l/h and 80% at 1.2 bar l/h [2]. The polarization process is based on the metastable spin exchange method. Typically transport cells of iron-free glass (Supremax glass, Schott, Mainz, Germany) with a volume of 1.2 L, were filled with 2.1–2.7 bars of 60–70% LP-^{3}He. Subsequently, the cells were placed in a shielded container with a low magnetic field (0.8 mT) produced by permanent magnets and transported to the MRI Laboratory in the Max Planck-Institute. The helium was then stored in a very homogeneous magnetic field of 2.5 mT, generated by five coaxial coils of 45 cm diameter and 70 cm total length. A gas mixing setup, similar to the one described in Ref. [9], allowed for a variation of the helium diffusion coefficient by admixing ^{3}He with a heavier buffer gas (here SF_6).

A phantom consisting of a distribution of long capillaries sketched in Fig. 2 was used in all the experiments. Single capillaries of radius $\tilde{R}_i$ = (0.25, 0.375, 0.7, 1.2, 1.6) mm (i = 1–5) were placed well apart in order to assure defined spatial resolution, while other capillaries with radius $\tilde{R}_2$ are grouped for purposes not relevant for this work. All capillaries were sealed at one end and placed inside a rubber tube of 6.4 mm radius. The space between the external part

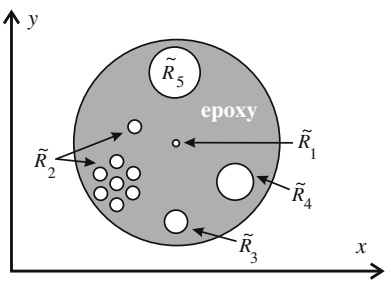

Fig. 2. Sketch of the phantom used, consisting of a set of parallel capillaries whose long axis is set parallel to the B_0 direction (z). The radii of the capillaries are $\tilde{R}_i$ = (0.25, 0.375, 0.7, 1.2, 1.6) mm (i = 1–5). Details on the construction of the phantom are given in the text.

of the capillaries and the rubber tube was filled with epoxy and left to dry. After the rubber tube is removed, the set of capillaries was cut to a length of 40 mm, which is longer than the rf coil used, and placed inside a glass tube of 6.5 mm radius and 150 mm length, provided with a valve at one end and sealed at the other. This glass container was fitted tightly into the rf coil by a Teflon spacer with its axis aligned parallel to the direction (z) of the static magnetic field (B_0) and with the valve-end attached to the gas handling system described in [9]. The glass container fulfills the dual function of connecting the phantom to the gas handling system while acting as a reservoir of LP-gas mixtures; the latter is due to the large amount of gas that is not affected by the rf-pulses [9,26–28].

2D images were acquired using a gradient echo FLASH Cartesian sampling of k-space. Fig. 1 shows a sketch of the pulse sequence and the timings used through the present work. The read gradient was set along the x direction in all experiments while the phase gradient was along the y direction. Tip angles of ~3° were achieved by means of a 5 μs rf-pulse. For the diffusion weighted experiments described below in Section 4.1 a read gradient of 87.6 mT/m was used. The signals were acquired with a spectral width of 50 kHz in a 32 × 32 matrix and zero filled to 128 × 128 points prior to FT. For the experiments of resolution enhancement described below in Section 4.2, gradients of 175.2 mT/m and a spectral width of 100 kHz were used. The 32 × 32 and 64 × 64 images were zero filled to four times their dimension before FT. In each experiment an FID was acquired immediately before each image acquisition and the data were normalized to the corresponding FID intensity before FT in order to take depolarization by rf excitation into account [9,26–28]. All images were acquired at essentially the same partial pressure for pure ^{3}He and are displayed normalized to their individual maxima.

4. Results

4.1. Diffusion weighted images

Fig. 3 shows a series of 2D images acquired as a function of the diffusion time, $\Delta = \delta$, for two different gas mixtures. The upper row corresponds to pure LP-^{3}He at 1 bar (Fig. 3a), with a free diffusion coefficient of $D_{He} = 1.8 \times 10^{-4}$ m^{2}s^{-1}, while the lower row corresponds to a binary mixture of 30% LP-^{3}He and 70% SF_6 (Fig. 3b) at 4 bars, with $D_{He/SF_6} = 1.7 \times 10^{-5}$ m^{2}s^{-1} [9] to allow for very similar partial pressures of ^{3}He. The diffusion times have a range of 0.32–2.32 ms and are detailed in the figure with increasing values from left to right. Around the phantom an exterior ring is visible due to gas which occupies the volume between the epoxy cylinder and the glass container. For short diffusion times all capillaries are clearly resolved. Even for the shortest diffusion time used, the effect of admixing a buffer gas should be appreciated from the contrast between different capillaries. In fact, the signal relations appear inverted, that is, bigger voids initially exhibit higher intensities than the smaller ones due to the lower ^{3}He diffusion. As $\Delta = \delta$ increases a smooth transition from a well resolved to a smeared image along the read direction is observed for capillaries $\tilde{R}_3$ to $\tilde{R}_5$, while the signal intensity of $\tilde{R}_1$ and $\tilde{R}_2$ remains almost constant. The effect is of course more noticeable when imaging pure ^{3}He. As the diffusion time increases, the same happens to the critical radius, while the distance, Δr, between spatially resolved structures decreases. When $\tilde{r}_c$ becomes larger than the image resolution, a helium molecule will diffuse a distance larger than the pixel size during the acquisition time. This behavior is explained in Fig. 4, where Δr and $\tilde{r}_c$ are plotted as a function of the diffusion time for both diffusion coefficients. The transition from well resolved to smeared image can be expected when the curve for Δr crosses the ones for $\tilde{r}_c$. This occurs for $\Delta = \delta \approx 0.5$ ms and

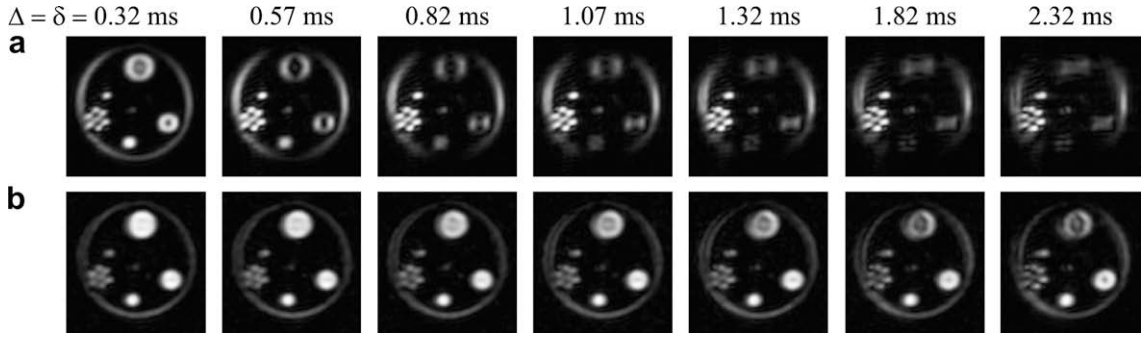

Fig. 3. 2D images as a function of Δ for pure ^{3}He (a) and for a 30% mixture of ^{3}He in SF_6 (b). From left to right the correspondent diffusion times are Δ = δ = 0.32, 0.57, 0.82, 1.07, 1.32, 1.82 and 2.32 ms using a read gradient of 87.6 mT/m. The exterior ring corresponds to free gas between the epoxy cylinder and the glass container. See text for details.

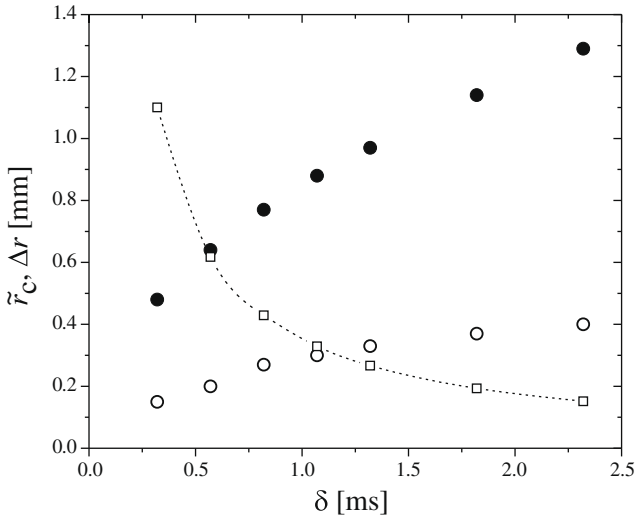

Fig. 4. Critical radius ($\tilde{r}_c$) for pure ^{3}He (closed symbols) and for the gas mixture (open symbols) as a function of δ (δ = Δ). Spatial resolution (Δr) is represented by small open square symbols connected by a line which serves as a guide for the eye.

Δ = δ ≈ 1 ms for pure helium and the gas mixture, respectively. These observations are also in accord with the smearing observed on the images shown in Fig. 3.

Another effect than can be observed is a transition from motional averaging to edge enhancement. Edge enhancement in a square slab containing ^{3}He has been reported in detail by Saam et al. [22]. Here we provide a descriptive analysis of the influence of sequence timing when imaging gases with different diffusion coefficients. Fig. 5 shows the profiles across the centers of $\tilde{R}_2$ to $\tilde{R}_5$ along the read direction for three values of Δ = δ. The behavior of $\tilde{R}_1$ is similar to that of $\tilde{R}_2$ and has been omitted from the figure for the sake of clarity. For this void size, the profile is essentially not altered, except for a decrease in amplitude due to diffusive attenuation. For pure ^{3}He a transition from a single resonance line for $\tilde{R}_3$, to a profile with pronounced edge enhancement takes place. As the diameter of the capillaries increases ($\tilde{R}_4$ and $\tilde{R}_5$) edge enhancement is always present. The decay of the amplitude in the center of each void is faster than on the edges due to diffusive attenuation. Notice that the third peak to the right of $\tilde{R}_4$ corresponds to gas in the gap between phantom and container (outer ring in the images). In the case of the gas mixture, diffusive effects are not significant enough to change the ratio of the signals from the edges and the center of each capillary, and an essentially static image is obtained. With increasing Δ = δ the intensity decays due to diffusion, and for $\tilde{R}_4$ and $\tilde{R}_5$ a change in the intensities of the edges and the centers of the capillaries becomes more evident.

Theoretical predictions by de Swiet [21] estimate a ratio of $l_s/l_g = 20$ for pure edge enhancement and $l_s/l_g = 2$ as the onset for the fast exchange or motional narrowing regime. For the experimental conditions presented in this work the ratios of l_s/l_g (with l_g = 399 μm for pure ^{3}He and l_g = 182 μm for the mixture) for the different capillaries are $(l_s/l_g)_i^{^3\mathrm{He}}$ = (1.3, 1.9, 3.5, 6.0, 8.0) and $(l_s/l_g)_i^{\mathrm{mix}}$ = (2.8, 4.2, 7.7, 13.2, 17.6) for i = 1–5, showing that the smaller and larger capillaries cover a broad range between strong to weak diffusion and should therefore show a distinct behavior. As Δ = δ increases, the shape of the profiles indicate motional narrowing for $\tilde{R}_2$ even for the larger value of Δ. $\tilde{R}_4$ and $\tilde{R}_5$ present strong edge enhancement, and with increasing Δ the center of the image decays more rapidly than the borders due to diffusion. The same effect has also been observed in MRI-experiments with ^{1}H [19] and LP-^{129}Xe [29].

Figs. 3–5 show that contrasts can be optimized not only by adjusting the pulse sequence to the diffusion time but also by controlling the diffusion coefficient of ^{3}He by the admixture of buffer gases. With reduced diffusion coefficient the distortions of the images are much smaller, and even the larger capillaries are clearly represented. Moreover, particularly for the larger capillaries, the enhanced sensitivity can lead to a resolution enhancement as described in the next section.

Finally the effect of the diffusion coefficient on the phase encoding direction is addressed. In the case of liquids with very low diffusion coefficients, the weak diffusion regime condition is generally fulfilled, giving rise to barely observable edge enhancement [19,21]. As discussed previously, for large diffusion coefficients the image will be a convolution with Gaussian function. For the intermediate values of D presented in Fig. 3 the effect of changing diffusion will be that of introducing different apodization functions to the data along the phase encoding direction. The experimental data in Fig. 3 behave accordingly.

4.2. Resolution enhancement

As previously discussed, admixing LP-^{3}He with buffer gases can greatly change the diffusion coefficient resulting in a sensitivity gain in unrestricted geometries [18]. Fig. 6 shows a set of images acquired with two different gas mixtures at two different spatial resolutions. For pure ^{3}He a 32 × 32 matrix recorded with a diffusion time of δ = Δ = 320 μs is shown in Fig. 6a, while the resulting image for a 64 × 64 matrix acquired with a diffusion time 2δ = 640 μs is shown in Fig. 6b. The longer diffusion time results in almost complete loss of signal from capillaries

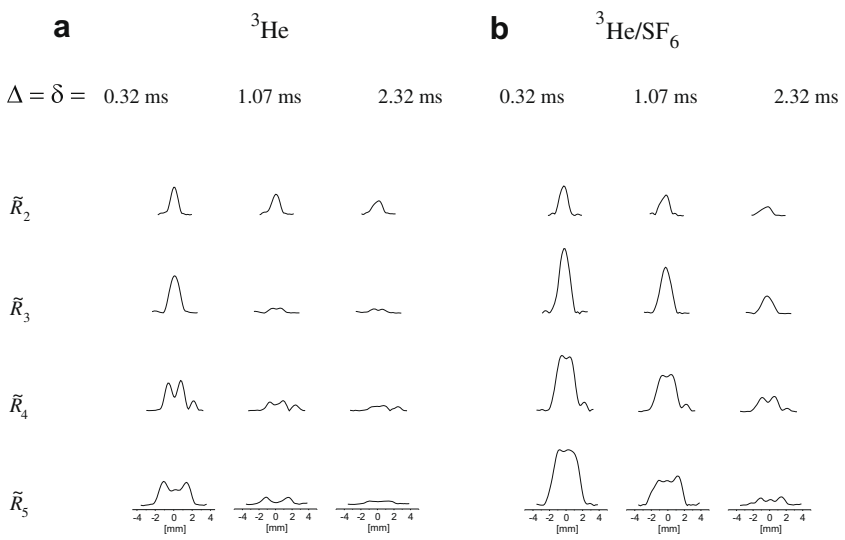

Fig. 5. Profiles of capillaries $\tilde{R}_2$ to $\tilde{R}_5$ taken from Fig. 3 for three different diffusion times, $\Delta = \delta = 0.32$, 1.07 and 2.32 ms for pure ^{3}He (a) and for the binary gas mixture ^{3}He/SF$_6$ (b).

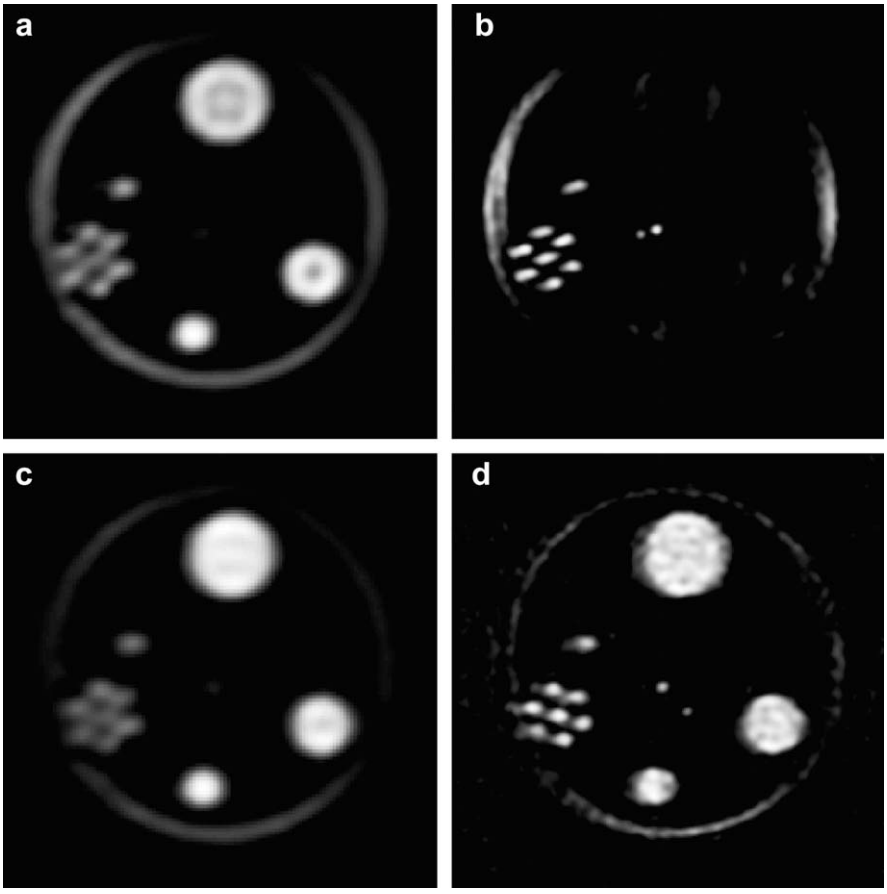

Fig. 6. Images showing resolution enhancement due to the reduction of the diffusion coefficient. Gradient intensity for read and phase direction $G = 175.2$ mT/m and spectral width 100 kHz. For pure ^{3}He: (a) 32×32 matrix, $\delta = 320$ μs (b) 64×64, $\delta = 640$ μs; and for the binary gas mixture (c) 32×32, $\delta = 320$ μs and (d) 64×64, $\delta = 640$ μs.

$\tilde{R}_3$ to $\tilde{R}_5$. A similar behavior is obtained if the timings are kept constant and the spectral width is doubled, requiring a factor 2 in gradient strength in order to keep same the FOV. The corresponding images for the binary gas mixture in Fig. 6c and 6d, demonstrate a remarkable gain in sensitivity for the larger capillaries. As already discussed in Eq. (3), the different void dimensions define a different ADC for each mixture, thus the signal attenuation due to diffusion in Eq. (5) for the different resolution can be written as (see Appendix)

$$\frac{S_{64}}{S_{32}} = \begin{cases} \exp\left(-\frac{1}{2}\gamma^2 G^2 \delta^2 \tilde{r}^2\right) & \text{for } \tilde{r} < \tilde{r}_c \\ \exp\left(-\frac{2}{3}\gamma^2 G^2 \delta^3 7 D_0\right) & \text{for } \tilde{r} > \tilde{r}_c \end{cases} \tag{7}$$

with δ for the 64×64 image being twice the value of the 32×32 image. The signal will be more attenuated as the radius of the cavity increases. For capillaries with a radius greater than $\tilde{r}_c$ the attenuation becomes constant. The mean attenuation ratio for the images shown in Fig. 6 is plotted in Fig. 7 as a function of the restriction dimension for both gas mixtures; the solid line corresponds to a Gaussian fit

$$\frac{S_{64}}{S_{32}}(\tilde{r}) = \exp\left(-\frac{\tilde{r}^2(\gamma G\delta)^2}{2}\right) + \exp\left(-\frac{2}{3}\gamma^2 G^2 \delta^3 7 D_0\right). \quad (8)$$

The width of the Gaussian fit for both mixtures is the same and matches the theoretical value within 10% accuracy. Again, the diffusion coefficient extracted from the fit of the baseline (second term in Eq. (8)) agrees with the theoretical values within 10% for the gas mixture and within 30% for pure ^{3}He. It should be noted that the description given by Eq. (8) is only a coarse approximation to the cylindrical shape of the capillaries and only applies for one gradient direction. A detailed description of the attenuation due to diffusion in cylindrical geometries is out of the scope of this paper and has been reported elsewhere [16]. Pure helium images show a slight attenuation for $\tilde{R}_1$ and the signal intensities rapidly decay to zero as the radius increases, whereas for the gas mixture, only a slight increase in sensitivity is observed for the smaller capillary and the attenuation stabilizes at a value of 0.5 with respect to the less resolved image.

5. Conclusions

In this work we have extended the use of buffer gases in LP-^{3}He MRI as a contrast agent for probing different sizes of spatial restriction. Mixing helium with a heavier buffer gas can be used to significantly reduce signal attenuation due to diffusion when sequences with long timings are required. A considerable gain in the SNR is obtained for large structures when the spatial resolution is increased, while sensitivity for smaller structures is not affected. Moreover, it should be noted that even though the discussion was centered on MRI, our results can also be applied to enhance sensitivity in any experiment that involves field gradients, such as probing restricted diffusion (q-space imaging) and flow in porous materials.

The implications of these findings for lung imaging are especially important, as this is by far the most extensive use of hyperpolarized gas MRI at the moment. Measurements of restricted diffusion in lungs involve mainly studies of lung emphysema. In this disease the alveolar walls become porous, leading to an increase of the ADC. An excellent review on the topic was recently provided by Conradi et al. [4,30]. In healthy human lungs each alveoli is an open vessel of approximately 300 μm in diameter. The diffusion coefficient of the mixture of ^{3}He at infinite dilution in N_2 has been measured to be around 0.8 cm^2/s. [9,31] and can be taken as the diffusion coefficient in the lung, as the helium concentration delivered to the patient is usually around 7% and probably close to infinite dilution when reaching the terminal structures. The typical duration of the gradient pulses used in clinical imaging are about 2 ms, giving rise to a root mean square displacement, in one dimension, of 0.6 mm. As this distance is much larger than the alveolar size, restricted diffusion will be present in healthy tissue, and will vary for a diseased lung. For example, in a study carried out on a number of healthy volunteers and patients with severe emphysema, the mean ADC was found to be around 0.2 cm^2/s and around 0.6 cm^2/s for healthy and for diseased lungs, respectively, [4]. If the diffusion coefficient of helium is decreased by admixture of a heavier buffer gas, it is not *a priori* clear whether LP-^{3}He imaging will still be useful to clearly distinguish between healthy and damaged tissue. The diffusion coefficient of ^{3}He in infinite dilution with SF_6 is 0.48 cm^2/s [9] giving rise to a root mean square displacement in one dimension of 0.4 mm for the same timings as before. This value still exceeds the average dimension of healthy alveoli. On the other hand, Conradi et al. have also shown that the distributions of ADCs using the much heavier perfluorinated gas C_3F_6 on excised healthy and diseased lungs displays clearly separated histograms with peaks on 0.017 cm^2/s for normal lungs and 0.032 cm^2/s for those with emphysema.

Hence it can be envisioned that the presented idea of admixing heavier buffer gases can become useful in clinical applications to increase spatial and/or temporal resolution without diminishing the diagnostic contrast as recently demonstrated in ^{3}He transport in rodent airways [32].

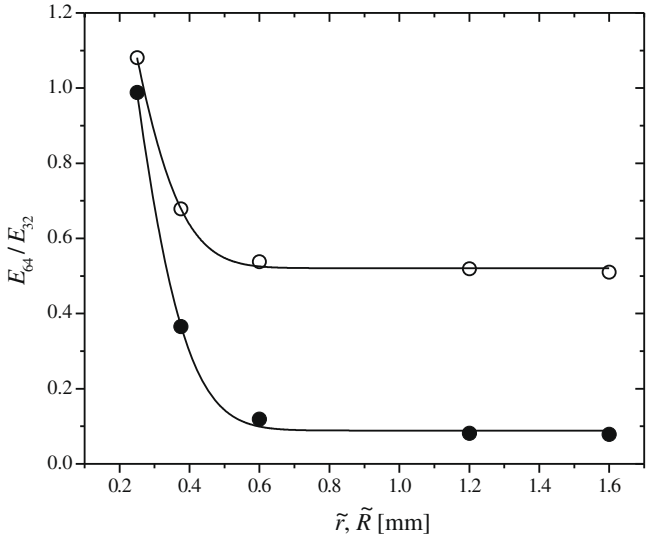

Fig. 7. Mean attenuation ratios for pure ^{3}He (closed circles) and for the gas mixture (open circles) images with different resolution shown in Fig. 6. Solid lines correspond to fits of Eq. (8) to the data.

Acknowledgments

The authors want to thank Manfred Hehn and Hanspeter Raich for their help in the design and construction of the gas handling system at the MPI-P and Jörg Schmiedeskamp for the ^{3}He hyperpolarization. Financial support by DFG (Forschergruppe *"Bildgestützte zeitliche und regionale Analyse der Ventilations – Perfusionsverhältnisse in der Lunge"*, grant # FOR 474) and a special grant of the Max Planck society made this work possible. Finally, we want to acknowledge the Partner Group for NMR Spectroscopy with High Spin Polarization FaMAF-MPIP.

Appendix

Derivation of equation (7)

The signal for $\Delta = \delta$ is given by Eq. (1) as $S(b) = S(0)\exp\left[-\frac{2}{3}\gamma^2 G^2 \delta^3 D\right]$. The duration δ of the read gradients for the image with 64 points is twice the one for 32 points $\delta_{64} = 2\delta_{32}$

Hence for $\tilde{r} < \tilde{r}_c$: The diffusion coefficient is given by Eq. (3) as $D = \frac{\tilde{r}^2}{4\delta}$ and

$$\frac{S_{64}}{S_{32}} = \frac{S(0)\exp\left[-\frac{2}{3}\gamma^2 G^2 \delta_{64}^3 \frac{\tilde{r}^2}{4\delta_{64}}\right]}{S(0)\exp\left[-\frac{2}{3}\gamma^2 G^2 \delta_{32}^3 \frac{\tilde{r}^2}{4\delta_{32}}\right]} = \exp\left[-\frac{1}{2}\gamma^2 G^2 \delta_{32}^2 \tilde{r}^2\right]$$

While for $\tilde{r} > \tilde{r}_c$: Eq. (3) defines $D = D_0$ and

$$\frac{S_{64}}{S_{32}} = \frac{S(0)\exp\left[-\frac{2}{3}\gamma^2 G^2 \delta_{64}^3 D_0\right]}{S(0)\exp\left[-\frac{2}{3}\gamma^2 G^2 \delta_{32}^3 D_0\right]} = \exp\left[-\frac{2}{3}\gamma^2 G^2 \delta_{32}^3 7 D_0\right]$$

Finally δ_{32} was replaced by δ.

References

[1] M. Wolf, Erzeugung höchster ^{3}He Kernspinpolarisation durch metastabiles optisches Pumpen, Physics, Johannes Gutenberg Universität, Mainz, 2004.

[2] E.J.R. van Beek, J. Schmiedeskamp, J.M. Wild, M.N.J. Paley, F. Filbir, S. Fichele, F. Knitz, G.H. Mills, N. Woodhouse, A. Swift, W. Heil, M. Wolf, E.W. Otten, Hyperpolarized 3-helium MR imaging of the lungs: testing the concept of a central production facility, Eur Radiol. 13 (2003) 2583–2586.

[3] B.M. Goodson, Nuclear magnetic resonance of laser-polarized noble gases in molecules, materials, and organisms, J. Magn. Reson. 155 (2002) 157–216.

[4] M.S. Conradi, B.T. Saam, D.A. Yablonskiy, J.C. Woods, Hyperpolarized ^{3}He and perfluorocarbon gas diffusion MRI of lungs, Prog. NMR Spect. 48 (2006) 63–83.

[5] P.T. Callaghan, Principles of Nuclear Magnetic Resonance Microscopy, Clarendon Press, Oxford, 1991.

[6] P.P. Zänker, J. Schmidt, J. Schmiedeskamp, R.H. Acosta, H.W. Spiess, Spin echo formation in the presence of stochastic dynamics, Phys. Rev. Lett. 99 (2007) 263001.

[7] W.S. Warren, Multidimensional symmetry in a three-dimensional world, Science 294 (2001) 1475–1476.

[8] P.P. Zänker, J. Schmiedeskamp, H.W. Spiess, R.H. Acosta, Distant dipolar fields in laser-polarized gases on macroscopic scales, Phys. Rev. Lett. 100 (2008) 213001.

[9] R.H. Acosta, L. Agulles-Pedrós, S. Komin, D. Sebastiani, H.W. Spiess, P. Blümler, Diffusion in binary gas mixtures studied by NMR of hyperpolarized gases and molecular dynamic simulations, Phys. Chem. Chem. Phys. 8 (2006) 4182–4188.

[10] H.E. Möller, X.J. Chen, B. Saam, K.D. Hagspiel, G.A. Johnson, T.A. Altes, E.E.d. Lange, H.-U. Kauczor, MRI of the lungs using hyperpolarized noble gases, Magn. Reson. Med. 47 (2002) 1029–1051.

[11] E.J.R. van Beek, J.M. Wild, H.-U. Kauczor, W.G. Schreiber, J.P. Mugler III, E.E.d. Lange, Functional MRI of the lung using hyperpolarized 3-helium gas, J. Magn. Reson. Imag. 20 (2004) 540–554.

[12] R.W. Mair, D.G. Cory, S. Peled, C.H. Tseng, S. Patz, R.L. Walsworth, Pulsed-field-gradient measurements of time-dependent gas diffusion, J. Magn. Reson. 135 (1998) 478–486.

[13] R.W. Mair, M.S. Rosen, R. Wang, D.G. Cory, R.L. Walsworth, Diffusion NMR methods applied to xenon gas for materials study, Magn. Reson. Chem. 40 (2002) S29–S39.

[14] R.W. Mair, M.N. Sen, M.D. Hurlimann, S. Patz, D.G. Cory, R.L. Walsworth, The narrow pulse approximation and long length scale determination in xenon gas diffusion NMR studies of model porous media, J. Magn. Reson. 156 (2002) 202–212.

[15] R.W. Mair, G.P. Wong, D. Hoffmann, M.D. Hürlimann, S. Patz, L.M. Schwartz, R.L. Walsworth, Probing porous media with gas diffusion NMR, Phys. Rev. Lett. 83 (1999) 3324–3327.

[16] R.H. Acosta, P. Blümler, L. Agulles-Pedrós, A.E. Morbach, J. Schmiedeskamp, A. Herweling, U. Wolf, A. Scholz, W.G. Schreiber, W. Heil, M. Thelen, H.W. Spiess, Controlling the diffusion of ^{3}He by buffer gases as a structural contrast agent in lung MRI, J. Magn. Reson. Imag. 24 (2006) 1291–1297.

[17] P. Blümler, R.H. Acosta, A. Thomas-Semm, S. Reuss, Lung fixation for the preservetion of air spaces, Exp. Lung Res. 30 (2004) 1–10.

[18] R.H. Acosta, P. Blümler, S. Han, S. Appelt, F.W. Häsing, J. Schmiedeskamp, W. Heil, H.W. Spiess, Imaging of a mixture of hyperpolarized ^{3}He and ^{129}Xe, Magn. Reson. Imag. 22 (2004) 1077–1083.

[19] P.T. Callaghan, A. Coy, L.C. Forde, C.J. Rofe, Diffusive relaxation and edge enhancement in NMR microscopy, J. Magn. Reson. A 101 (1993) 347–350.

[20] T.M. de Swiet, P.N. Sen, Decay of nuclear magnetization by bounded diffusion in a constant field gradient, J. Chem. Phys. 100 (1994) 5597–5604.

[21] T.M.d. Swiet, Diffusive edge enhancement in imaging, J. Magn. Reson. B 109 (1995) 12–18.

[22] B.T. Saam, N. Drukker, W. Happer, Edge enhancement observed with hyperpolarized ^{3}He, Chem. Phys. Lett. 263 (1996) 481–487.

[23] E.O. Stejskal, J.E. Tanner, Spin diffusion measurements: spin echoes in the presence of a time-dependent field gradient, J. Chem. Phys. 42 (1965) 288.

[24] P.P. Mitra, M.N. Sen, L.M. Schwartz, P. Le Doussal, Diffusion propagator as a probe of the structure of porous media, Phys. Rev. Lett. 68 (1992) 3555–3558.

[25] M. Carl, G.W. Miller, J.P. Mugler III, S. Rohrbaugh, W.A. Tobias, G.D. Cates Jr., Measurement of hyperpolarized gas diffusion at very short time scales, J. Magn. Reson. 189 (2007) 228–240.

[26] H.E. Möller, X.J. Chen, M.S. Chawla, B. Driehuys, L.W. Hedlund, G.A. Johnson, Signal dynamics in magnetic resonance imaging of the lung with hyperpolarized noble gases, J. Magn. Reson. 135 (1998) 133–143.

[27] J.-H. Gao, L. Lemen, J. Xiong, B. Paytal, P.T. Fox, Magnetization and diffusion effects in NMR imaging of hyperpolarized substances, Magn. Reson. Med. 37 (1997) 153–158.

[28] G.A. Johnson, G. Cates, X.J. Chen, G.P. Cofer, B. Driehuys, W. Happer, L.W. Hedlund, B. Saam, M.D. Shattuck, J. Swartz, Dynamics of magnetization in hyperpolarized gas MRI of the lung, Magn. Reson. Med. 38 (1997) 66–71.

[29] Yi-Qiao Song, Boyd M. Goodson, Bhima Sheridan, T.M.d. Swiet, A. Pines, Effects of diffusion on magnetic resonance imaging of laser-polarized xenon gas, J. Chem. Phys. 108 (1998) 6233–6239.

[30] B.T. Saam, D.A. Yablonskiy, V.D. Kodibagkar, J.C. Leawoods, D.S. Gierada, J.D. Cooper, S.S. Lefrak, M.S. Conradi, MR imaging of diffusion of ^{3}He gas in healthy and diseased lungs, Magnet. Reson. Med. 44 (2000) 174–179.

[31] D.A. Yablonskiy, A.L. Sukstanskii, J.C. Leawoods, D.S. Gierada, G.L. Bretthorst, S.S. Lefrak, J.D. Cooper, M.S. Conradi, Quantitative in vivo assessment of lung microstructure at the alveolar level with hyperpolarized ^{3}He diffusion MRI, Proc. Natl. Acad. Sci. USA 99 (2002).

[32] K.R. Minard, R.E. Jacob, G. Laicher, D.R. Einstein, A.P. Kuprat, R.A. Corley, MR imaging of apparent ^{3}He gas transport in narrow pipes and rodent airways, J. Magn. Reson. 194 (2008) 182–191.